Effects of Uniaxial Compression on the Third-Zone Fermi Surface of Aluminum*

W. A. Spurgeon and D. Lazarus
Department of Physics and Materials Research Laboratory, University of Illinois, Urbana, Illinois 61801
(Received 31 July 1972)

The effects of uniaxial compression up to 40 kg/cm^2 on the areas of the [110]-γ and [100]-β orbits of the third-zone Fermi surface of aluminum have been determined by means of a de Haas–van Alphen phase-shift technique. Both areas were found to increase under compression, the γ-orbit area by $(4.6 \pm 0.3) \times 10^{-3}\%/(\text{kg/cm}^2)$ and the β-orbit area by $(3.4 \pm 0.7) \times 10^{-3}\%/(\text{kg/cm}^2)$. The estimates of the errors allow for the possibility of systematic errors. The nearly-free-electron (NFE) and four-orthogonalized-plane-waves (OPW) models for the aluminum Fermi surface were used to calculate the effects of uniaxial compression, hydrostatic pressure, and alloying on the γ and β cross sections. The NFE results for both orbits were not at all satisfactory. The predictions of the four OPW model for the stress and pressure derivatives of the γ-orbit area agreed with experiment within the experimental error when the changes in the matrix elements with stress and pressure were obtained from the q dependence of the Heine–Abarenkov form factor. The dependence on alloying, calculated from the four-OPW model on the assumption that the change in matrix elements and volume was negligible, was in equally good agreement with experiment. The results of similar four-OPW calculations for the β orbit did not agree with experiment quite so well, the discrepancies being roughly twice as large as the experimental error.

I. INTRODUCTION

Knowledge of the Fermi surfaces of metals has been greatly expanded in the past decade. The Fermi surfaces of the readily available simple metals and even many of the more complex transition metals have been mapped out in considerable detail by a variety of methods. Theoretical understanding has also improved, and Fermi surfaces calculated from appropriate models can be made to agree with experiment to within one percent or better. It is important to test these models under changes in scale by calculating and measuring the effects on the Fermi surface of hydrostatic and uniaxial strains and of alloying.

Different information is obtained from each of these three perturbations. Hydrostatic pressure changes only the volume of a (cubic) crystal. A uniaxial stress will produce a small volume change, but its major effect is to change the lattice symmetry. Alloying changes the concentration of conduction electrons primarily, while changing the volume and symmetry of the crystal only very slightly. A complete understanding of the electronic structure of a metal must include an understanding of the effects of these perturbations.

Aluminum is a particularly good choice for such a study. It is a face-centered-cubic metal which is light enough for the conduction electrons to have very little d character. The Fermi surface and its dependence on the above perturbations should thus be fairly easy to calculate. The Fermi surface has a number of rather small pieces which are very sensitive to the choice of parameters used in the theoretical fit and also to perturbations. The metal is also easy to work with experimentally, and all three perturbations can be applied.

The experimentally determined aluminum Fermi surface[1,2] bears a well-known qualitative resemblance to that predicted by the familiar nearly-free-electron (NFE) model.[3] Important quantitative (and also some qualitative) discrepancies with experiment remain in the NFE model, however, particularly in regard to the third zone section (Fig. 1). On this section, the strength of the periodic potential of the lattice has a large effect and a multiple-orthogonalized-plane-wave (OPW) model must be used to remove these discrepancies. In order to obtain rapid convergence in the multiple-OPW model, the actual lattice potential is replaced by a pseudopotential. The theoretical justification for this procedure and a discussion of the multiple-OPW model in general can be found in a number of texts.[3-5]

At least four plane waves must be used to describe the aluminum Fermi surface in the vicinity of the corner W of the Brillouin zone, since three Bragg reflection planes intersect at this point. The Fermi surface is determined from the equation

$$\begin{vmatrix} \vec{k}_1^2 - E_F & w_2 & w_1 & w_1 \\ w_2 & \vec{k}_2^2 - E_F & w_1 & w_1 \\ w_1 & w_1 & \vec{k}_3^2 - E_F & w_2 \\ w_1 & w_1 & w_2 & \vec{k}_4^2 - E_F \end{vmatrix} = 0 , \qquad (1)$$

where $\vec{k}_i^2$ is the kinetic energy of the ith plane wave, E_F is the Fermi energy, and w_1 and w_2 are

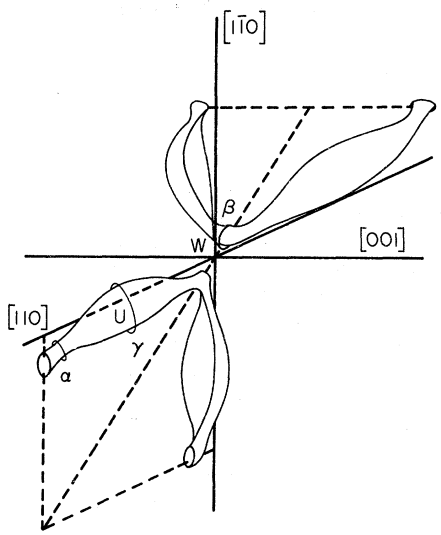

FIG. 1. A portion of the third-zone Fermi surface of aluminum. The γ and β orbits are indicated.

the matrix elements of the pseudopotential for plane waves differing by $2\pi/a[1, 1, 1]$ and $2\pi/a[0, 0, 2]$ (a is the lattice parameter and units such that $\hbar^2/2m = 1$ have been adopted). Values of the parameters E_F, w_1, and w_2 which, together with Eq. (1), excellently reproduce the experimental aluminum Fermi surface have been obtained by Ashcroft[6] and by Anderson and Lane.[2] Both calculations were performed using four plane waves throughout the minimal symmetry element of the Brillouin zone.

In addition to having been mapped out in detail by means of the de Haas–van Alphen (dHvA) effect and fitted with a four-OPW model, portions of the third-zone Fermi surface of aluminum have been studied under pressure and in dilute alloys. Melz[7] has found the γ- and β-orbit areas (Fig. 1) to change by $(-0.47 \pm 0.06)\%$/kbar and $+(1.2 \pm 0.15)\%$/kbar, respectively. In their experiment on dilute alloys of aluminum, Shepherd and Gordon[8] and Abele and Blatt[9] found the areas to depend only on N_e, the effective number of conduction electrons. For a 0.33% decrease in N_e, corresponding to a 1-at.% zinc alloy, for example, the area of the γ orbit decreased by about $(7.0 \pm 1.5)\%$, whereas the β-orbit area decreased by $(32 \pm 3)\%$.

The purpose of the present experiment is to study the effects of uniaxial stress on the third-zone Fermi surface by means of a dHvA phase-shift method. The [110]-γ and [100]-β orbits are the preferred candidates for this study because they are perhaps the two most important orbits to be considered in the theoretical fit, because they are small enough for the stress effects to be large, because they are relatively unchanged by a rotation of the sample in the field, and because they have been previously studied under pressure and in dilute alloys. The experiment and its results and limitations are discussed in Sec. II. In Sec. III the NFE and four-OPW models for the third-zone Fermi surface are extended to obtain theoretical predictions for the stress, pressure, and alloy dependence of the orbits, using various models to calculate the change in the pseudopotential matrix elements.

II. EXPERIMENTAL METHODS AND RESULTS

A. Sample Preparation

Samples were spark cut from a large single crystal of nominally 99.9999% pure aluminum obtained from Cominco Products, Inc., Spokane, Washington. Most of the samples were 0.18 in. square by 0.5 in. long. The ratio of resistance at 300 and 4.2 °K, measured by Melz[7] on other samples cut from the same crystal, was 6300. The spark-cut samples were mounted for polishing in an aluminum block with phenylsalicytate. Careful mounting ensured that the rectangular parallelopiped shape of the samples was not altered by the polishing. The polishing was done on granite blocks using successively 25-, 1-, and 0.05-μ alumina, and finally cheese-cloth abrasives. The samples were polished until their ends were as flat and smooth as possible and parallel to within 10 μ (as measured by a capacitance method).

B. Apparatus

The dHvA signals were detected by a field-modulation technique, using a Varian 40-kG superconducting solenoid with 10^{-5} field homogeneity to provide the static magnetic field. The theory and practice of dHvA spectroscopy by this method have been treated in detail by Stark and Windmiller.[10] Details of the coil assembly are shown in Fig. 2.

Detected dHvA signals were typically about 5–10 μV at the pickup coils. For the γ orbit these signals were obtained at approximately 25 kG at 4.2 °K. The β-orbit signals were considerably weaker, and it was necessary to reduce the temperature to about 1.6 °K at approximately 8.5 kG to detect them adequately. The β-orbit signals were stronger at higher fields, but the γ-orbit signals were strong enough to cause unwanted interference at fields above 9.5 kG. Typical results for the γ and β oscillations are shown in Figs. 3 and 4. A modulating frequency of 105 Hz was used in taking most of the data, although 25 Hz modulation was used occasionally to test the homogeneity of the strain. The dHvA signals were detected at the second harmonic of the modulating frequency.

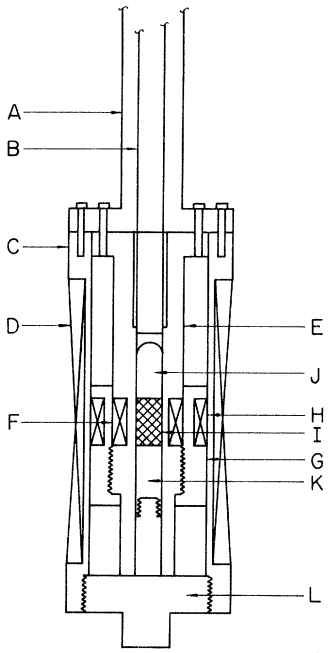

FIG. 2. Coil form assembly: A, support from top to probe; B, stainless-steel plunger; C, beryllium-copper form for modulating coil; D, modulating coil (2000 turns, No. 30 copper wire); E, nylon form for pickup coil No. 2; F, pickup coil No. 1 (4000 turns, No. 38 copper wire); G, nylon form for pickup coil No. 2; H, pickup coil No. 2 (approximately 1300 turns, No. 34 copper wire); I, sample; J, fired lavite plug with hemispherical boss; K, fired lavite support for sample; L, beryllium-copper support for sample.

C. Noise

Aside from some distortions of the signal, to be discussed later along with other possible sources of systematic error, the major source of noise in the experiment was microphonics. A significant reduction in the microphonic noise was achieved by using concentric series-opposed balanced pickup coils as described by Stark and Windmiller.[10] It was also found necessary to isolate the magnet from the floor. This was done by placing the magnet on a platform constructed in layers, from the bottom up, of $\frac{1}{4}$-in. thick rubber, $\frac{3}{4}$-in. thick plywood, and 1-in. thick stainless steel. The resulting improvement in signal-to-noise ratio was quite noticeable.

D. Stresses

The samples were stressed by direct loading with calibrated weights through a long plunger and a highly polished fired lavite plug. This plug had a hemispherical boss to help ensure a uniaxial stress. The bottom support for the sample was also made of highly polished fired lavite, which provided strength and a very low friction surface. The plunger was brought out of the Dewar through a Teflon spacer, and could fall freely for short distances. For the experiment on the β orbit it was necessary to pump to 1.6 °K. Therefore a large vacuum can was placed over the top of the probe to keep air from being cryopumped into the Dewar, which could freeze the plunger in place. The weights were tied together in a manner such that they could be raised or lowered individually through a seal at the top of the can. The stress was applied parallel to the field in both cases, i.e., parallel to [110] for the γ orbit and parallel to [100] for the β orbit.

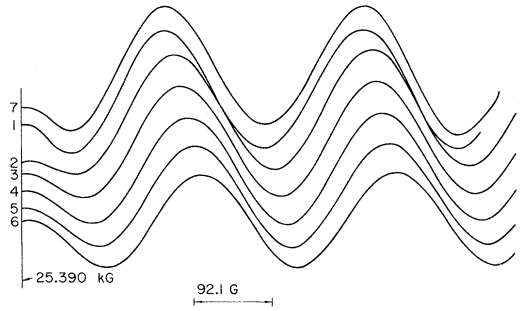

FIG. 3. Sample of the γ-orbit data. Stress is measured in kg/cm^2. Curve 1, 0 stress; curve 2, 9.1 stress; curve 3, 15.5 stress; curve 4, 21.8 stress; curve 5, 27.1 stress; curve 6, 34.2 stress; curve 7, 0 stress (repeat of curve 1 after loading).

E. Measurement Procedure

The uniaxial stress which can be applied to an aluminum single crystal without introducing plastic deformation is not very large; typical strains must be $\lesssim 10^{-4}$. Even if the effect of the stress

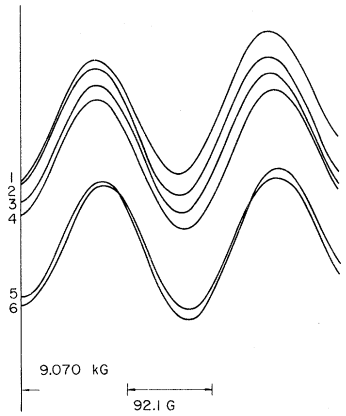

FIG. 4. Sample of the β-orbit data. Stress is measured in kg/cm^2. Curves 1 and 2, 0 stress; curves 3 and 4, 12.5 stress; curves 5 and 6, 37.6 stress.

were large it would probably be difficult to determine the stress effect by a direct measurement of the dHvA frequency under stress. It is therefore best to measure the change in frequency directly by means of a phase-shift technique.[11] If F' and F are the frequencies with and without stress, the dHvA oscillations will have the same phase ϕ at different values of field (H' and H), where

$$\phi = 2\pi F/H + \beta = 2\pi F'/H' + \beta. \quad (2)$$

(The constant β is assumed to be unchanged by stress.) To find the difference in field, $H - H'$, the oscillations with and without stress are recorded on the same grid (as in Figs. 3 and 4) on which vertical lines correspond to constant values of field. The change in field for constant phase is easily measured. If $F' = F + \delta F$ and $H' = H + \delta H$, then $\delta F/F = \delta H/H$. Since the frequency and area A of the external orbit in question are related by the Onsager relation, $2\pi F = \hbar c A/e$, we obtain $\delta F/F = \delta A/A$, where δA is the area change.

In practice we measure the current in the magnet rather than the field, and plot this on the horizontal axis as in Figs. 3 and 4. The current-field relationship is sufficiently well known that this procedure introduces negligible errors. To be able to measure small changes in the current, a mercury cell zero offset was provided for the recorder. A sufficiently slow and resettable field sweep was also required. This was provided by driving a ten-turn helipot connected in parallel with the fine control helipot in the magnet power supply by means of a low speed motor. The frequency shifts did not depend on the direction of the field sweep. However, the field lags the current in the magnet during a sweep, so all measurements during a given loading cycle were made with the field swept in only one direction for internal consistency. Most of the data were taken with increasing increments of stress, although no definite difference between runs taken with increasing and decreasing stress could be detected. The zero stress curve was usually repeated after each loading cycle, and reproducibility was generally excellent. The minimum frequency changes which could be reliably detected were about $(4\times10^{-3})\%$ for the γ orbit and $(2\times10^{-2})\%$ for the β orbit.

Data were taken over several loading cycles for each sample. The high sensitivity of the γ orbit to stress permitted the use of small and numerous increments of stress. For the β orbit only four values of stress were used, but the curves corresponding to each value were usually repeated several times to improve accuracy. The frequency shifts were measured over two or three oscillations and averaged for each value of stress. These results were then plotted as a function of stress and fitted to a straight line by the method of least squares. An example of this reduction of the raw data is shown in Fig. 5. The averaging decreased the scatter in the data, and hopefully helped to minimize any systematic error from the distorted signals.

F. Results

Reproducibility between samples was poor until the polishing technique previously described was adopted. The results for the good samples (those which were polished in the accepted manner and which did not have distorted signals) are presented in Table I. Samples L_1 through L_6 were $\frac{1}{2}$ in. long, whereas sample S_1 was $\frac{1}{4}$ in. long. The average frequency changes were $[4.6\pm0.2\,(2\sigma)]\times10^{-3}\%/(\mathrm{kg/cm^2})$ for the γ orbit and $[3.4\pm0.2\,(2\sigma)]\times10^{-3}\%/(\mathrm{kg/cm^2})$ for the β orbit. Given the ample possibility of small systematic errors, and the small frequency changes for the β orbit, the β orbit results are probably reliable to $\pm20\%$ and the γ orbit results to $\pm8\%$ of the stated values.

G. Systematic Errors

Signal distortions can introduce systematic errors in the results. An example of these distorted signals is shown in Fig. 6. At times, the signals were only minimally (if at all) distorted, and at other times, under seemingly identical operating conditions, the signals were so poor that no reliable data could be taken. The results shown in Figs. 3 and 6, for example, were taken on similarly prepared samples on successive days. The

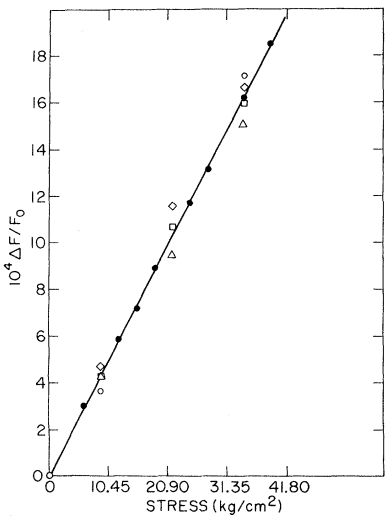

FIG. 5. Reduction of γ-orbit data. The open figures correspond to values obtained at different extrema of the oscillations shown in Fig. 4. The solid circles are the average value of the frequency change obtained using all the data for this particular sample. The solid line is the least-squares fit to the average values.

origin of the signal distortion was not completely certain. The two most likely possibilities seem to be flux trapping by the superconducting solenoid and inhomogeneities in the strain in the samples. Both were probably responsible to some extent.

Small scale flux trapping would disrupt the magnet current-magnetic-field relationship and hence distort the signal. Seasoning the solenoid by sweeping it back and forth through large field ranges occasionally seemed to help. Some seasoning of the magnet was always done before data were taken, and a field region in which the signals were minimally distorted was selected for data taking.

The samples could also be composed of domains of varying strain (possibly introduced in the polishing or spark-cutting operations), and the dHvA signals from each domain could have a slightly different phase. If the average dHvA phase in the sample is ϕ, and the phase in the ith domain differs from ϕ by an amount α_i, the amplitude A_i of the total signal will be given by

$$A=\sum_i A_i \sin(\phi+\alpha_i)\,, \tag{3}$$

where A_i is the amplitude for the ith domain. This expression can be rewritten as

$$A=\sum_i A_i \sin\phi\cos\alpha_i+\sum_i A_i \cos\phi\sin\alpha_i\,. \tag{4}$$

The first term in this expression is the desired signal. It is, however, diminished from the ideal amplitude by the $\cos\alpha_i$ factors. The second term is a distortion in the signal. An additional external stress changes ϕ and the α_i as well. The amplitude of the signal could then show a stress dependence and the shapes of the signals could also be altered by the stress.

The scatter in the results was appreciable and the frequency change was sometimes a nonlinear function of stress when the signal distortion was

TABLE I. Stress dependence of third-zone orbits.

Sample	$\delta A/A$ [units of 10^{-3}%/(kg/cm^2)]
γ-orbit results	
L_1	4.55
L_2	4.70
L_3	4.77
L_4	4.77
S_1	4.31
β-orbit results	
L_5	3.64
L_6	3.54
L_7	3.23
L_8	3.35

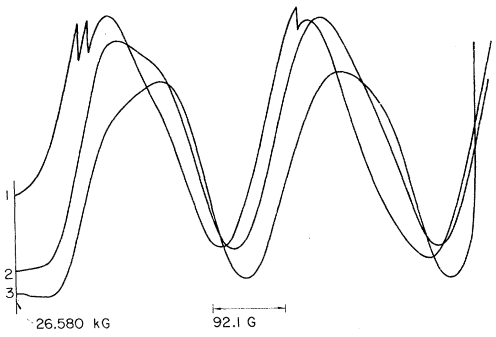

FIG. 6. Example of the signal distortion. Stress is measured in kg/cm^2. Curve 1, 0 stress, curve 2, 18.6 stress; curve 3, 38.7 stress.

large. If the signals from a given sample were badly distorted, the results were regarded as unreliable and discarded. If the distortion was minimal, the effects of the α_i's were minimized by considering the peaks of the oscillations as the points of constant phase. The second term is small in this case, since $\cos\phi$ is approximately zero. The averaging procedure previously described will further reduce the scatter in the results. It should be noted that the amplitudes of the oscillations were somewhat stress dependent, even when the distortion was not significant. Usually the stress decreased the amplitudes, sometimes by as much as 30%, although increases were occasionally observed.

There are a number of possible sources of systematic error in this experiment besides those arising from the signal distortion. First, it is possible to change the observed dHvA frequency by rotating the sample in the field. This error would be largest for the γ orbit where, for rotation in a (110) plane, the frequency depends on the rotation angle θ measured from [110], as $F=F_{110}(1+\frac{1}{2}\theta^2)$ for small θ.[6] If the sample were rotated by one degree relative to the field by the application of maximum stress, an error of 8% in the frequency change would result. However, the coil assembly was a sufficiently tight fit in the Dewar that a rotation of even a quarter of a degree was improbable. The curves of the β-orbit frequency for rotation in both (110) and (100) planes are sufficiently flat within 5° of [100] that any contributions to the frequency change from rotating the sample would be insignificant.

Another possible source of error is a displacement of the sample relative to the field when stress is applied. The field was homogeneous to 1 part in 10^5 in the region occupied by the sample, and the sample was fairly well constrained from such displacements, so a maximum change of 5 parts in 10^5 of the average field at the sample was un-

likely. Even this change corresponds to an error in the frequency change of only 2.5% for the γ orbit and 3.8% for the β orbit.

Plastic deformation is another possible but unlikely source of systematic error. The maximum stress used (40 kg/cm^2) was well below the stress required for slip. All data were taken after the samples had been prestressed slightly above the maximum stress used for data taking. The excellent reproducibility of the zero stress curves before and after a loading cycle strongly suggests that only elastic strains were involved in all runs.

A more serious source of systematic error is the lack of knowledge of the actual strain in the crystal. The force applied to the sample was measured, whereas the strain in the sample had to be calculated from the elastic constants on the assumption that the sample deformed properly under the load. This assumption would not be valid if the polished ends of the sample were not parallel, if the sample were a nonrectangular parallelopiped, if the sample bowed under stress, or if barreling occurred to any significant extent. With the exception of a bowing deformation, which requires a very large stress, it is nearly impossible to completely eliminate these problems.

Careful polishing of the samples should ensure that they are in the proper rectangular parallelopiped shape. This was confirmed by examination of the samples under a low-power microscope. Some of the samples prepared before the final polishing technique was established were not in this shape, and the distortion was observable by careful examination with the naked eye. The stress derivatives found for the γ orbit with these samples were often far too large, and reproducibility of the results between these samples was poor. Reproducibility of the results improved appreciably after the final polishing technique was adopted. An improperly shaped sample will be subjected to a shear by the load, which will cause the transverse strains to be too large. This effect would lead to too large a stress derivative, particularly for the γ orbit.

The possibility of a barreling distortion is harder to evaluate. The contact between the polished ends of the sample and the lavite ends of the stressing apparatus is not perfectly frictionless. The ends of the sample are thus slightly constrained from expanding under the stress, whereas the central portions of the sample are not, and the sample can become barrel shaped. The strain in the sample will be smaller than it should be and will not be completely homogeneous. In consequence, the stress derivatives will be too small, and the amplitudes of the oscillations might show an appreciable stress dependence. Careful polishing of the samples will minimize this friction but not eliminate it.

The effects of barreling will be considerably more important in a short sample than in a longer one with the same cross section, so a short ($\frac{1}{4}$ in. long) sample (sample S_1) was run to test for barreling. The amplitude of the γ oscillations for this sample decreased by about 20% with maximum stress, and the stress derivative was $(4.31\times10^{-3})\%/(\mathrm{kg/cm^2})$, which is about 8% lower than the average found for the $\frac{1}{2}$-in.-long specimens. Initially it was thought that this difference could be due to barreling. The stress dependence of the β orbit could not be measured well enough to provide a good test for barreling.

The barreling problem can be solved for the worst possible case, in which the ends of the sample are completely constrained from expanding laterally. A solution to this problem has been published by Filon.[12] His numerical results for the radial strain of a cylindrical sample of radius a and length $2c$ for the case $\pi a = 3c$ are shown in Fig. 7. This choice of dimensions corresponds roughly to the short sample case. Values of the radial strain for the case $\pi a = c$, corresponding roughly to the long sample dimensions, were worked out using Filon's equations and are also shown in Fig. 7. Considering the scaling of the barreling with sample length for the worst possible case, it is probable that the difference between the short and long sample results would have been much greater had barreling been a serious problem.

Data were taken at both 25 and 105 Hz on another sample to provide a check of the homogeneity of the strain. At 105 Hz the outer 25% of the sample was within one skin depth of the surface whereas 50% of the sample was within this region at 25 Hz. The results for the γ oscillation stress derivative of $(4.93\times10^{-3})\%/(\mathrm{kg/cm^2})$ at 25 Hz and $(4.77\times10^{-3})\%/(\mathrm{kg/cm^2})$ at 105 Hz agree well within the 8% experimental error. This sample was found to be misshapen after the experiment, however, so the stress derivatives were not included in the

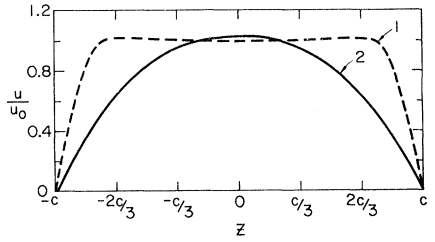

FIG. 7. Radial elongation under extreme barreling conditions. The radial elongation is normalized to the ideal value (u_0). Curve 1, $\pi a = c$ (long sample); curve 2, $\pi a = 3c$ (short sample).

final analysis.

In all, the systematic errors are thought to have been fairly well minimized. Nevertheless, the standard deviation of the results is probably not a true indication of their reliability. A more conservative estimate of their reliability is ±8% for the γ-orbit stress derivative and ±20% for the β-orbit stress derivative.

III. COMPARISON WITH THEORY

A. γ Orbit

The NFE approximation provides the simplest model from which we can calculate the stress dependence of the aluminum Fermi surface. This approximation predicts an area for the γ orbit which is about twice as large as the actual area (Fig. 8), so we would not expect quantitative agreement with the measured stress derivative. The NFE result is important, however, because the NFE model is a strictly geometrical model which is the basis of the multiple-OPW model. A straightforward calculation yields a prediction of an area increase of $(2.14\times10^{-3})\%/(\mathrm{kg/cm^2})$. This is about 45% of the experimental value of $(4.6\times10^{-3})\%/(\mathrm{kg/cm^2})$, hence the change in the area of the orbit with stress is largely a consequence of the change in geometry.

We must calculate the γ-orbit stress derivative from a four-OPW model to obtain quantitative agreement with experiment. As mentioned in Sec. I, the four-OPW Fermi surface is obtained from Eq. (1):

$$\begin{vmatrix} \vec{k}_1^2 - E_F & w_2 & w_1 & w_1 \\ w_2 & \vec{k}_2^2 - E_F & w_1 & w_1 \\ w_1 & w_1 & \vec{k}_3^2 - E_F & w_2 \\ w_1 & w_1 & w_2 & \vec{k}_4^2 - E_F \end{vmatrix} = 0 .$$

It is convenient to write the wave vectors in terms of displacements from the symmetry point U:

$$\begin{aligned} \vec{k}_1 &= [\tfrac{1}{4}, \tfrac{1}{4}, 1] + (1/\sqrt{2})[1, 1, 0]x \\ &\quad + (1/\sqrt{2})[-1, 1, 0]y + [0, 0, 1]z , \\ \vec{k}_2 &= \vec{k}_1 - [0, 0, 2] , \\ \vec{k}_3 &= \vec{k}_1 - [1, 1, 1] , \\ \vec{k}_4 &= \vec{k}_1 - [-1, 1, 1] . \end{aligned} \tag{5}$$

The orbit is obtained by solving Eq. (1) for z as a function of x for a $y=0$ cross section.

The effects of a uniaxial stress are easy to include in the four-OPW model, and for a crystal stress along [1, 1, 0] Eq. (1) becomes

$$\begin{vmatrix} (\vec{k}_1 + \vec{\delta k}_1)^2 - (E_F + \delta E_F) & w_2 + c & w_1 + a & w_1 + b \\ w_2 + c & (\vec{k}_2 + \vec{\delta k}_2)^2 - (E_F + \delta E_F) & w_1 + a & w_1 + b \\ w_1 + a & w_1 + a & (\vec{k}_3 + \vec{\delta k}_3)^2 - (E_F + \delta E_F) & w_2 + d \\ w_1 + b & w_1 + b & w_2 + d & (\vec{k}_4 + \vec{\delta k}_4)^2 - (E_F + \delta E_F) \end{vmatrix} = 0 . \tag{6}$$

The changes in the wave vectors $\vec{\delta k}_i$ are readily determined from the elastic constants.[13] Since the difference between the four-OPW and NFE values for E_F is very small (0.85685 and 0.86057 Ry, respectively[6]), and since the changes in the pseudopotential matrix elements are expected to be small, δE_F should be the same as the NFE value to a very good approximation. The changes in the pseudopotential matrix elements (a, b, c, and d) must be determined from a model for the pseudopotential, for which we now consider several possibilities.

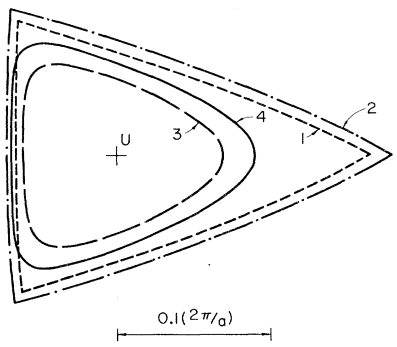

FIG. 8. The NFE and four-OPW γ orbits. Curve 1, NFE, $T=0$; curve 2, NFE, $T=10^4$ kg/cm^2; curve 3, four-OPW, $T=0$; curve 4, four-OPW, $T=10^4$ kg/cm^2.

The NFE model suggests that most of the change in area is a consequence of the geometry change. As a reasonable first approximation, then, consider the matrix elements to be unchanged with stress. Equation (6) leads to a stress derivative of $(3.45\times10^{-3})\%/(\mathrm{kg/cm^2})$, which is about 25% too small. Some change in the pseudopotential matrix elements is evidently needed.

The change in the matrix elements might be found from a simple point-ion potential for which a formula is easily obtained. This potential consists of a Coulombic attraction to the ion core and a δ-function repulsion at the nucleus, both of which are considered to be screened. The equation for the

form factor is

$$w(q) = (-4\pi Ze^2/q^2 + \beta)/\Omega\epsilon(q), \quad (7)$$

where Ω is the atomic volume and $\epsilon(q)$ is the Hartree dielectric function.[14] This form factor is plotted as a function of q/k_f in Fig. 9. The parameter β can be chosen in various ways. Taking $\beta = 43.8$ Ry/atomic unit of volume, sets $w(q)$ equal to zero for $q/k_f \cong 1.41$, consistent with Harrison's "OPW" form factor.[15] A uniaxial stress will change the values of q for which Bragg reflection planes exist as well as the volume of the crystal. Values for the changes in the matrix elements were calculated from this form factor on the assumption that β remains unchanged. These values (listed in Table II) together with Eq. (6) lead to a stress derivative of $(5.0\times10^{-3})\%/(\text{kg/cm}^2)$, which is nearly within the experimental error. It should be noted that the values of w_1 and w_2 predicted for this model for the pseudopotential are far too large, so only the changes in the matrix elements predicted by the model were used in all calculations based on this model.

A better pseudopotential has been devised by Heine and Abarenkov.[16] Physically, their model replaces the actual potential by a Coulomb potential outside a sphere of radius R_M, and by an energy- and angular-momentum-dependent square well inside of this sphere. The form factor for this model potential is plotted in Fig. 9. The agreement with Ashcroft's values for the matrix elements ($w_1 = 0.0179$ Ry and $w_2 = 0.0562$ Ry) is quite good. This form factor can be represented by a relation of the form $w(q) = f(q)/\Omega$, and the changes in the matrix elements can be found in a straightforward manner. These values, together with Eq. (6) lead to an area increase of $(4.50\times10^{-3})\%/(\text{kg/cm}^2)$, which is satisfactorily within the experimental error.

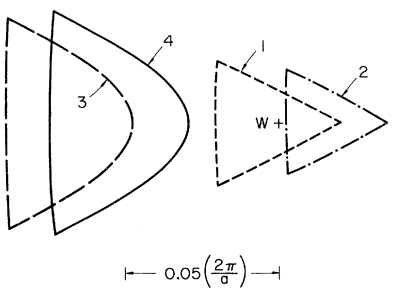

FIG. 9. Comparison of the Harrison point-ion and Heine–Abarenkov pseudopotential form factors. The Harrison point-ion form factor (open circles) was computed from the formula $w(\vec{q}) = (-4\pi ze^2/q^2 + \beta)/\Omega\epsilon(\vec{q})$, with $\beta = 43.8$ Ry/atomic unit of volume, using a Hartree dielectric function for $\epsilon(\vec{q})$.

TABLE II. Summary of four-OPW calculations.

γ-orbit stress derivatives[a]					
a	b	c	d	$\delta A/A_0$	Model
0	0	0	0	3.45	
−0.00282	0.00517	−0.00078	0.000122	4.5	Heine–Abarenkov
−0.00353	0.00657	−0.00193	0.00235	5.0	Point ion
β-orbit stress derivatives[a]					
a'	b'	c'	$\delta A/A_0$		Model
0	0	0	−0.65		
0.000602	−0.00078	0.00320	1.8		Heine–Abarenkov
0.000713	−0.00193	0.00692	4.4		Point ion
Pressure derivatives[b]					
a	b	$(\delta A/A_0)\gamma$	$(\delta A/A_0)\beta$		Model
0.00167	0.00152	−0.41	1.48		Heine–Abarenkov
0.00216	0.00253	−0.70	1.77		Point ion

[a] $\delta A/A_0$ is in units of $10^{-3}\%/(\text{kg/cm}^2)$ and matrix element changes are in units of $\text{Ry}/10^4\ \text{kg/cm}^2$.

[b] $\delta A/A_0$ is in units of %/kbar and matrix element changes are in units of Ry/10 kbars.

The four-OPW γ-orbit stress derivative can thus be made to agree quite well with experiment. The result is not very sensitive to the choice of pseudopotential, although some change in the pseudopotential matrix elements is needed to explain the result. The calculations described above were performed using Ashcroft's parameters as a basis. The results of all calculations using Anderson and Lane's parameters as a basis agreed with those obtained using Ashcroft's parameters as a basis within the estimated computational errors (3% of the calculated values for the γ-orbit derivatives). The areas in stressed aluminum were calculated for a stress of 10^4 kg/cm^2 in order to keep the computational error small. The four-OPW γ orbits for stressed and unstressed aluminum are shown in Fig. 8.

The pressure derivative of the γ-orbit area can also be calculated from Eq. (6) ($a = b$ and $c = d$ in this case). The changes in the wave vectors were obtained from the elastic constants and the change in E_F from the NFE model as before. Use of the q dependence of the Heine–Abarenkov form factor for the changes in the matrix elements leads to an area change of -0.41%/kbar. This value is in satisfactory agreement with Melz's experimental value of $(-0.47\pm0.06)\%$/kbar. In a somewhat more involved calculation based on the four-OPW model, Hepfer and Rayne[17] obtained a pressure derivative of -0.43%/kbar. The matrix element changes predicted by the Heine–Abarenkov model were used in their calculations.

The γ-orbit pressure derivative is more sensitive to the model for the pseudopotential than is the stress derivative. The point-ion potential with $\beta = 43.8$ Ry/atomic unit of volume leads to a pressure derivative of -0.70%/kbar, for example. It should be noted that the NFE model, which predicts an area increase of 0.074%/kbar, is entirely

inadequate for this calculation.

A satisfactory fit to the γ-orbit alloy dependence can be obtained from the equation

$$\delta A = \left.\frac{\partial A}{\partial E}\right|_{E_F} \delta E_F , \tag{8}$$

in which δE_F derives entirely from the change in effective number of conduction electrons N_e and $\partial A/\partial E|_{E_F}$ is obtained from the band structure effective mass.[8,9] This procedure is equivalent to calculating the area change directly from the four-OPW model with no change in the matrix elements and neglecting any change in the wave vectors and Fermi energy arising from the small volume change. The result is an area decrease of 7.0% for a 0.33% decrease in N_e. (Shepherd and Gordon[8] show a calculated value of -7.7%, but a 7.0% decrease is not a worse fit to their data.) The effects of the volume change can be estimated from the pressure dependence and the room temperature changes of the lattice constant with alloying.[18] Including these effects would lead to a 6% decrease for a 1% magnesium alloy and a 7.3% decrease for a 1% zinc alloy. The data are not adequate to detect these differences. The NFE result, an area decrease of 4.6% for a 0.33% change in N_e, is definitely too small, however.

All of the γ-orbit data can thus be well explained by the four-OPW model. There are several additional potential sources of difficulty which should be mentioned. First of all, the matrix elements obtained by Ashcroft and by Anderson and Lane should be regarded as matrix elements of the form $\bar{w}(\vec{q})$, defined by the relation

$$\bar{w}(\vec{q}) = w(\vec{q}) + \sum_{\vec{q}\neq\vec{q}'} \frac{w(\vec{q}-\vec{q}')w(\vec{q}')}{E(\vec{q})-E(\vec{q}')} , \tag{9}$$

where $\vec{q}$ and $\vec{q}'$ are reciprocal lattice vectors.[19] It is not entirely clear whether the change in matrix elements calculated from the various models (in particular, the Heine–Abarenkov model) should be regarded as more appropriate for w or $\bar{w}$ matrix elements. They were used as $\bar{w}$ matrix elements for better or worse. For the stress dependence this makes little difference since the stress dependence was not very sensitive to the choice of pseudopotential. The difference might be more important for the pressure dependence, although the fit based on the Heine–Abarenkov model is satisfactory.

The matrix elements could also be $\vec{k}$ dependent, but this effect should be of minimal importance for an orbit as NFE-like as the γ. The energy dependence of the matrix elements arising from the energy dependence of the square well in the Heine–Abarenkov model could be of some importance in calculating the pressure and alloy dependence, but should be unimportant in calculating the stress dependence, since the change in Fermi energy is very small. There is also some question of whether the volume dependence of the screening is adequately treated by the Heine–Abarenkov model as used here. The data are not adequate for a definitive test for these effects, which are expected to be small in any event.

B. β Orbit

The NFE model successfully predicted the sign and order of magnitude of the γ orbit stress derivative. This model predicts a stress derivative of $(-3.3\times10^{-3})\%/(\mathrm{kg/cm^2})$ for the β orbit which is nearly the opposite of the experimental value. The change in the pseudopotential matrix elements with stress thus dominates the geometrical changes in determining the β-orbit stress derivative, and we must turn to the four-OPW model in order to correctly predict even the sign of the stress derivative. This is hardly surprising considering the major differences between the NFE and four-OPW β orbits (Fig. 10).

The four-OPW secular equation for an aluminum crystal compressed along [010] can be written as

$$\begin{vmatrix} (\vec{k}_1+\vec{\delta}k_1)^2-(E_F+\delta E_F) & w_2+b' & w_1+a' & w_1+a' \\ w_2+b' & (\vec{k}_2+\vec{\delta}k_2)^2-(E_F+\delta E_F) & w_1+a' & w_1+a' \\ w_1+a' & w_1+a' & (\vec{k}_3+\vec{\delta}k_3)^2-(E_F+\delta E_F) & w_2+c' \\ w_1+a' & w_1+a' & w_2+c' & (\vec{k}_4+\vec{\delta}k_4)^2-(E_F+\delta E_F) \end{vmatrix} = 0 . \tag{10}$$

The $\vec{k}_i$ are now most conveniently written in terms of departures from the symmetry point W; for example,

$$\vec{k}_1 = [\tfrac{1}{2},\ 0,\ 1] + [1,\ 0,\ 0]x + [0,\ 1,\ 0]y + [0,\ 0,\ 1]z . \tag{11}$$

The β orbit is obtained by solving for z as a function of x for the $y=0$ cross section. The changes in wave vectors, Fermi energy, and matrix elements with stress were obtained in the same manner as for the γ orbit.

For no change in the matrix elements, Eq. (10) leads to a β-orbit stress derivative of $(-0.6\times10^{-3})\%/(\mathrm{kg/cm^2})$. This is still of the wrong sign, although it is a definite improvement over the NFE result. A much improved result of $(1.8\times10^{-3})\%/$

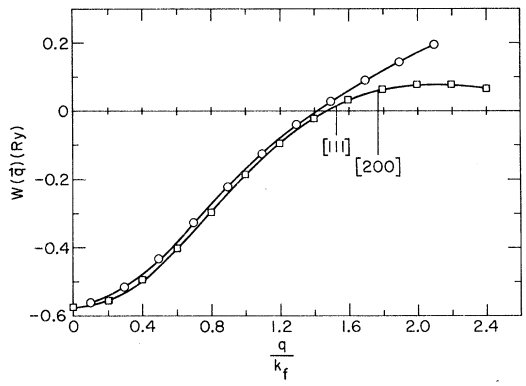

FIG. 10. NFE and four-OPW β orbits. Curve 1, NFE, $T=0$; curve 2, NFE, $T=10^4$ kg/cm^2; curve 3, four-OPW, $T=0$; curve 4, four-OPW, $T=10^4$ kg/cm^2.

(kg/cm^2) is obtained when the changes in the matrix elements are found from the q dependence of the Heine–Abarenkov form factor. Although the result is 45% too low, it is at least of the proper sign and order of magnitude. Finally, the point-ion potential leads to a stress derivative of (4.4×10^{-3})%/(kg/cm^2), which is slightly larger than the experimental value plus the experimental error. The possible computational error is estimated to be about 5% of the calculated derivatives of the β-orbit area.

The pressure dependence of the β orbit can be calculated in the same manner as for the γ orbit. Use of the Heine–Abarenkov model for the change in matrix elements leads to an area increase of 1.48%/kbar, which is not far from Melz's experimental value of (1.20 ± 0.15)%/kbar. The result of Hepfer and Rayne's calculation was 1.37%/kbar. Use of the point-ion potential for the changes in matrix elements results in an area increase of 1.77%/kbar. The NFE result, an area increase of 0.074%/kbar, is inadequate, as it was for the γ orbit.

The dependence of the β orbit on alloying calculated from Eq. (9) using Ashcroft's value for the band structure effective mass[6] is a 32% decrease in area for an 0.33% decrease in N_e. The result calculated from the four-OPW model on the assumptions of no change in the matrix elements and neglecting any volume effects is an area decrease of 27% for the same decrease in N_e. The difference probably arises from a small energy dependence of the matrix elements that Ashcroft assumed in his calculations of the effective mass. The 32% decrease is clearly a better fit to the experimental data. The NFE result, an area decrease of 22%, is too small.

Small orbits such as the β orbit are in general very sensitive to the effects of the pseudopotential. The effects of the difference between w and $\bar{w}$ matrix elements and the $\vec{k}$ and energy dependence of the matrix elements will accordingly be more important in calculating the β-orbit derivatives than for calculating the γ-orbit derivatives. Unfortunately, it is not simple to include these details in the calculations, but the results of the calculations based on the point-ion potential should represent an upper bound to their importance.

It should be noted that a slightly larger change in the matrix elements than that predicted by the Heine–Abarenkov model as used here would improve the calculated stress derivative for the β orbit without changing the calculated γ-orbit stress derivative much. A similar increase in the change in w_2 would also improve the fit to both pressure derivatives. Considering the high sensitivity of the γ orbit and the relative simplicity of the four-OPW model, the agreement between theory and experiment for the β-orbit results is reasonably satisfactory. However, in view of the recent work of Van Dyke,[20] agreement with the four-OPW model may well be fortuitous.

IV. SUMMARY

The stress dependence of the γ and β orbits of the aluminum third-zone Fermi surface was measured by means of a de Haas–van Alphen phase-shift technique. The γ- and β-orbit areas increased by $(4.6\pm0.3)\times10^{-3}$% and $(3.4\pm0.7)\times10^{-3}$%/(kg/cm^2), respectively, under compression. The estimated errors are fairly conservative to allow for the possibility of systematic errors.

A four-OPW model was used to calculate the dependence of the orbits on uniaxial stress, hydrostatic pressure, and alloying. The calculated results for the γ orbit agreed with experiment within the experimental error when the changes in the pseudopotential matrix elements were obtained from the Heine–Abarenkov model for the pseudopotential or, in the case of the alloy dependence, were assumed to be zero. Discrepancies roughly twice as large as the experimental error remained in similar four-OPW calculations for the β orbit. In all, the four-OPW model provided a reasonably satisfactory, if possibly fortuitous, explanation for the dependence of the two orbits on uniaxial stress, hydrostatic pressure, and alloying.

*Work supported in part by the U. S. Atomic Energy Commission under Contract No. AT(11-1)-1198.

[1]C. O. Larson and W. L. Gordon, Phys. Rev. 156, 703 (1967).

[2]J. R. Anderson and S. S. Lane, Phys. Rev. B 2, 298 (1970).

[3]W. A. Harrison, *Pseudopotentials in the Theory of Metals* (Benjamin, New York, 1966).

[4]*Solid State Physics*, edited by H. Ehrenreich, F. Seitz, and D. Turnbull (Academic, New York, 1970), Vol. 24.
[5]V. Heine, in *The Physics of Metals, Vol. 1, Electrons*, edited by J. M. Ziman (Cambridge U. P., London, 1969), p. 1.
[6]N. W. Ashcroft, Phil. Mag. 8, 2055 (1963).
[7]P. J. Melz, Phys. Rev. 152, 540 (1966).
[8]J. P. G. Shepherd and W. L. Gordon, Phys. Rev. 169, 541 (1968).
[9]J. C. Abele and F. J. Blatt, Phys. Rev. B 1, 1298 (1970).
[10]R. W. Stark and L. R. Windmiller, Cryogenics 8, 272 (1968).
[11]D. Shoenberg and B. R. Watts, Phil. Mag. 15, 1275 (1967); J. E. Schirber and W. J. O'Sullivan, Phys. Rev. 184, 628 (1969); I. M. Templeton, Proc. Roy. Soc. (London) A292, 413 (1966).
[12]L. N. G. Filon, Trans. Roy. Soc. London Ser. A 198, 155 (1902).
[13]C. Kittel, *Introduction to Solid State Physics*, 3rd ed. (Wiley, New York, 1966), p. 122.
[14]W. A. Harrison, Ref. 3, p. 49.
[15]W. A. Harrison, Ref. 3, p. 33.
[16]A. E. O. Animalu and V. Heine, Phil. Mag. 12, 1249 (1965).
[17]K. C. Hepfer and J. A. Rayne, Phys. Rev. B 4, 1050 (1971).
[18]W. B. Pearson, *Handbook of Lattice Spacings and Structures of Metals* (Pergamon, New York, 1964), p. 346.
[19]M. L. Cohen and V. Heine, in Ref. 4, p. 78.
[20]J. P. Van Dyke, Bull. Am. Phys. Soc. 17, 324 (1972); 17, 694 (1972).

PHYSICAL REVIEW B VOLUME 6, NUMBER 12 15 DECEMBER 1972

Magnetic Surface States in Cadmium*

J. P. Rahn, J. J. Sabo, Jr., and J. E. Weir
Department of Physics, University of Washington, Seattle, Washington 98105
(Received 7 June 1972)

Presented here are the first systematic measurements of the low-field (0–80-Oe) microwave surface impedance of cadmium. The surface impedance is dominated by transitions between magnetic surface states. The magnetic fields at which these transitions occur were measured as a function of the orientation of the magnetic field in the three principal crystal planes of cadmium. Five distinct series are presented and the ratios of the observed transition fields agree with the Prange–Nee theory. These series are assigned to points on the Fermi surface and the Fermi velocities on the third-band lens are presented.

I. INTRODUCTION

The purpose of this paper is to report the results of an extensive experimental investigation and analysis of the cadmium magnetic-surface-states spectra as a function of sample orientation. These low-field surface-impedance oscillations were first reported by Khaikin[1] in 1960 and were later studied experimentally by Koch and Kuo.[2] They reported two features of the surface-resistance-derivative maxima that were uniquely different from cyclotron resonance. First, the magnetic fields of the maxima scaled as $\omega_{rf}^{3/2}$ (where ω_{rf} is the microwave field frequency), in contrast to cyclotron resonance where the magnetic fields scaled as ω_{rf}. Second, no great loss of signal occurred when the field was tipped out of the surface of the sample. In 1968 Prange and Nee[3] proposed an elegant mechanism to explain the low-field oscillations. They proposed that the electrons which participate in the low-field power absorption are those which are reflected specularly from the surface of the metal and repeat identical skipping orbits in the microwave skin depth. Since at these very low magnetic fields a skip subtends a very small arc, the electrons which are responsible for the low-field oscillatory surface impedance are located on a narrow band near $v_z = 0$ on the Fermi surface, where v_z is the velocity normal to the surface of the metal. They also suggested that the point on this band where the resonance parameter is stationary with respect to the momentum parallel to the magnetic field, k_H, will contribute most strongly to the resonance. Since the Nee–Prange theory was published, Koch and his collaborators[4–7] have experimentally confirmed many aspects of the theory. Mathematically, the electrons involved are magnetically induced quantum surface states. Prange and Nee solved the Schrödinger equation for electrons in a potential well formed on one side by the essentially infinite surface potential of the crystal and on the other side by the nearly linear attractive potential due to the magnetic field. From the resulting wave functions and energy eigenvalues, they calculated the surface impedance. The equation[4] giving the magnetic field H_{mn}, at which the $m \rightarrow n$ transition occurs, is

$$H_{mn} = \omega_{rf}^{3/2}(c\hbar/e)(a_m - a_n)^{-3/2}(2K_\perp/v_\perp^3)^{1/2}, \qquad (1)$$

where a_m is the mth negative root of the Airy function Ai(z). Here $K_\perp$ is the radius of curvature of the electron's orbit in k space at the resonance